ELSEVIER

Superlattices and Microstructures 33 (2003) 311–337

Superlattices and Microstructures

www.elsevier.com/locate/jnlabr/yspmi

Optical transmission and reflection spectroscopy of single quantum dots

Khaled Karrai[a,*], Richard J. Warburton[b]

[a] *Center for NanoScience and Sektion Physik der Ludwig-Maximilians-Universität, Geschwister-Scholl-Platz 1, 80539 Munich, Germany*

[b] *School of Engineering and Physical Sciences, Heriot-Watt University, Edinburgh EH14 4AS, UK*

Accepted 5 February 2004

Abstract

An analytical formulation of the interband optical transmission and reflectivity spectra of a single quantum dot embedded in a semiconductor is presented. We consider the effect of the sample surface as well as other reflecting surfaces on the shape of the spectra near the ground state exciton resonance. The saturation of the transmission and reflectivity spectra due to the quantum optical saturation of the transition at higher light power is presented.

A quantum dot, very much like an atom, absorbs or scatters light at discrete optical frequencies [1–3]. The scattering is resonant when the photon energy matches an exciton energy level [4]. A recent development has been the detection of these resonances in individual dots using optical transmission and reflection experiments. These experiments use tunable lasers with narrow spectral lines [5–9]. In the existing literature, the analysis of the transmission spectra is very simplified in that the effect of the sample surface and other interfaces close to the dots has been ignored. Furthermore, the non-linear effects inherent to the saturation of the absorption at high optical power have also been neglected. In this paper we present a model with which we derive expressions for the single dot transmission and reflection coefficients. We consider realistic samples containing quantum dots as can be grown by self-assembly in molecular beam epitaxy. We include the effects of the sample surface, and extend these to the case of a quantum dot interacting with a tunable

* Corresponding author. Fax: +49-89-2180-3182.
E-mail address: khaled.karrai@lmu.de (K. Karrai).

0749-6036/$ - see front matter © 2004 Elsevier Ltd. All rights reserved.
doi:10.1016/j.spmi.2004.02.007

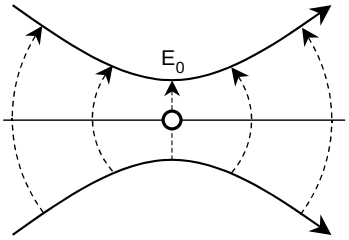

Fig. 1. Schematic view of a dot in the beam of a focused laser spot. This represents a transmission experiment. The electric components of the optical driving fields are shown. The dot is positioned in the region with the narrowest beam waist.

Fabry–Perot resonator. We point out that the excitonic optical transition in a single quantum dot saturates at very modest power densities, and based on the two-level approximation, we calculate the non-linear behavior of the absorption coefficient as a function of the light power.

1. Transmission and reflectivity in the weak absorption limit

In one experimental arrangement designed to measure the optical properties of a single quantum dot, a high numerical aperture objective lens focuses a collimated laser beam down to a diffraction limited Gaussian spot size [7, 8]. This geometry has the advantage over nano-optical techniques involving sub-wavelength apertures that the intensity profile of the probing beam is very well known. We assume that the probing spot is centered over a single quantum dot. In a classical description, the dot is polarizable and can be driven into resonance by the electric component $\vec{E}_0$ of the light. The dot responds by emitting an electromagnetic field with strength $\vec{E}_T$. In a carefully designed transmission experiment, the detector should collect the transmitted light in a solid angle corresponding to the numerical aperture of the illuminating objective. When measuring the reflectivity, the back-scattered light can be collected with the objective lens which matches naturally the illumination and reflectivity solid angles. In transmission, the photo signal is proportional to $|\vec{E}_0 + \vec{E}_T|^2$, and in reflectivity, the photo signal is proportional to $|\vec{E}_R|^2$ where we assume at this stage that the dot is embedded in a homogeneous medium with optical index n, far from any reflecting surface. This is obviously not a realistic case for most solid state quantum dots which are typically located within a few hundred nanometers from the surface. Nevertheless, we use this idealization as a necessary staring point, including subsequently the effects of a free surface. At this stage we also assume that the light intensity is low enough that the dot remains in the linear response regime. In order to evaluate the transmission and reflection coefficients of the dot, we need to calculate the forward-scattered and back-scattered fields, respectively,

$$\vec{E}_T = \vec{E}_0 + \vec{E}_S \qquad \text{and} \qquad \vec{E}_R = \vec{E}_S, \tag{1}$$

where E_S is the amplitude of the scattered field. Fig. 1 shows that the dot experiences a

driving field with a flat phase front over the area A of the focused spot. In this situation, the dot is excited essentially by a quasi plane wave with one dot per unit area A. This is a reasonable assumption considering that tightly focused spots are orders of magnitude larger than the dot itself.

We use the optical theorem [10] to relate the total amount of forward-scattered light to the field scattered along the direction of the impinging plane wave. The problem is now identical to that of the optical transmission and reflectivity of an infinite plane of uniformly distributed identical quantum dots with an areal density $1/A$. The field of such an oscillating two-dimensional dipole system is given by [11],

$$\vec{E}_S = \frac{1}{A}\frac{e}{2\varepsilon_0 cn}\ddot{\vec{r}}(t - z/c), \tag{2}$$

showing that we need to calculate the time derivative of the dipole oscillation amplitude r. The distance z is the distance to the plane of dots. This formula is correct for all z, even in the near-field when $z \ll \lambda$ [11]. The discrete spectrum of the dot's excitonic resonances is included in the frequency response of the dipole. A semi-classical analysis of the dot's response gives,

$$\vec{r} = -\frac{e\vec{E}_0}{m_0}\sum_k \frac{f_k}{\omega_k^2 - \omega^2 - i\omega\Gamma_k}, \tag{3}$$

where f_k is the oscillator strength of the resonance at angular frequency ω_k, and Γ_k is the corresponding dephasing rate for that resonance. For simplicity we will consider here only the ground state resonance ω_0 with a dephasing rate Γ and an oscillator strength f. If more than one optical transition has to be considered, the model can be easily extended using the full summation given in the formula above. In order to calculate the time derivative of the dipole oscillation amplitude, we consider an electromagnetic driving field with amplitude E_0 and time-dependence $\exp(-i\omega t)$, in which case,

$$\ddot{\vec{r}} = \frac{ef\vec{E}_0}{m_0}\frac{i\omega}{\omega_0^2 - \omega^2 - i\omega\Gamma}. \tag{4}$$

This implies that the scattered field E_S is now,

$$\vec{E}_S = \frac{1}{A}\frac{e^2 f}{2\varepsilon_0 c m_0 n}\frac{i\omega}{\omega_0^2 - \omega^2 - i\omega\Gamma}\vec{E}_0. \tag{5}$$

This expression can be conveniently simplified considering the realistic case of sharp exciton resonances for which $\Gamma \ll \omega_0$, giving,

$$\vec{E}_S = \frac{\alpha_0}{2}\frac{-i\gamma}{\delta + i\gamma}\vec{E}_0, \tag{6}$$

where

$$\delta = \omega - \omega_0, \tag{7}$$

is the detuning (the angular frequency measured from the resonance), and γ is half the dephasing rate,

$$\gamma = \Gamma/2. \tag{8}$$

The constant α_0 is given by,

$$\alpha_0 = \frac{1}{A}\frac{e^2 f}{\varepsilon_0 c m_0 n \Gamma}, \tag{9}$$

which, as we will see shortly, is the absorption at the resonance. The oscillator strength can be related to the optical dipole moment μ_{12} of the excitonic transition [12],

$$f = \frac{2m_0\omega_0}{\hbar}\left(\frac{\mu_{12}}{e}\right)^2. \tag{10}$$

Numerically this corresponds to,

$$f = 26.2\hbar\omega \text{ (in eV)} \{(\mu_{12}/e) \text{ in nm}\}^2, \tag{11}$$

or equivalently,

$$(\mu_{12}/e) \text{ (in nm)} = 0.195\{f/\hbar\omega \text{ (in eV)}\}^{1/2}. \tag{12}$$

For example, for a self-assembled InAs dot grown by molecular beam epitaxy, we have determined $f = 11.8$ at photon energy $\hbar\omega = 1.28$ eV. This corresponds to $\mu_{12}/e = 0.59$ nm. Several papers refer to the dipole moment in units of Debye [5, 6] where 1 Debye $= 3.335\,64 \times 10^{-30}$ C m. In the above example, the dipole moment corresponds to $\mu_{12} = 28.4$ Debye. The reason f is considerably larger than 1 arises because the dipole is part of a semiconductor matrix. Without electron–hole correlations, the oscillator strength can be related to the Kane matrix element E_p. E_p describes the strength of the dipole coupling between the s- and p-atomic orbitals. Assuming a perfect overlap of the electron and hole wave functions in the quantum dot, the result is $f = E_p/2\hbar\omega$ [4]. E_p is almost the same for InAs and GaAs; taking the GaAs value (25.7 eV), the prediction is that $f = 10.0$ for $\hbar\omega = 1.28$ eV, in good agreement with the experimental result. Electron and hole correlations increase the oscillator strength and although they play a modest role for self-assembled quantum dots, they increase the oscillator strength for so-called natural quantum dots [5, 6].

An important point is that the product,

$$\alpha_0\gamma = \frac{1}{A}\frac{e^2 f}{2\varepsilon_0 c m_0 n} = \frac{1}{A}\frac{\hbar\omega_0\mu_{12}^2}{\hbar^2\varepsilon_0 n c}, \tag{13}$$

is a direct measure of the dipole moment of the exciton. This is true independent of the dephasing rate and therefore also independent of the dephasing mechanism. This product can be directly determined from resonant transmission spectra, yielding a direct measurement of the dipole moment.

Experimentally, one measures the transmission and reflectivity coefficients given by,

$$T = \left|\frac{E_0 + E_S}{E_0}\right|^2 \qquad \text{and} \qquad R = \left|\frac{E_S}{E_0}\right|^2. \tag{14}$$

Using the expression for the scattered field, we find that,

$$T = \left(1 - \frac{\alpha_0}{2}\frac{\gamma^2}{\delta^2+\gamma^2}\right)^2 + \left(\frac{\alpha_0}{2}\frac{\gamma\delta}{\delta^2+\gamma^2}\right)^2, \qquad \text{and} \tag{15}$$

$$R = \left(\frac{\alpha_0}{2}\frac{\gamma^2}{\delta^2+\gamma^2}\right)^2. \tag{16}$$

In presently existing experiments [5–9], the scattering is weak, i.e. $\alpha_0 \ll 1$, in which case the expression for the transmission simplifies further to,

$$T \cong 1 - \alpha_0\frac{\gamma^2}{\delta^2+\gamma^2}, \tag{17}$$

where it is now obvious that α_0 is the maximum contrast ΔT in the transmission spectrum. The resonance lineshape is a Lorentzian with a full width at half maximum (FWHM) of $\Gamma = 2\gamma$. It is important to note that the corresponding result for the reflectivity with these assumptions implies that the maximum contrast of the dot reflectivity is $\Delta R = (\alpha_0/2)^2$, a factor $\alpha_0/2$ smaller than ΔT. This has dramatic consequences. For instance, in our experiments [8] α_0 was typically of the order of 10^{-3}, implying a reflectivity contrast of just 5×10^{-7} which would be extremely difficult to measure. The contrast in transmission is much higher than in reflectivity because the transmitted field is a coherent superposition of the driving laser field with the forward-scattered field. Such a superposition is equivalent to a homodyne detection. In this sense, a transmission measurement has an automatically in-built homodyne detection. This homodyne detection is clearly absent in the case of the back-scattered field assuming, as we have done throughout so far, that the dot is completely buried in a homogeneous semiconductor. However, a homodyne detection can be included also in the reflectivity measurement by superposing coherently the back-scattered field with a reference driving light field. This can be achieved in practice simply by using the surface of the semiconductor to give a reference back-scattered beam. This has an advantage over the transmission because the phase of the scattered field relative to the reference field can easily be tuned, allowing interferometry to be carried out on a single quantum dot. In general, since the dot is almost always located near the sample surface, the reflectivity is strongly influenced by the sample surface, a case we consider in detail in Section 4.

2. Radiation damping

The dephasing rate determines the FWHM of the resonance of the transmission described in Eq. (17). The fundamental limit to the exciton dephasing is given by the radiation damping. In this case, dephasing occurs when the exciton relaxes by spontaneously emitting a photon. The dephasing rate is then given by [11, 13, 14],

$$\Gamma_{sp} = 2\gamma_{sp} = \frac{2\pi}{3(\lambda/n)^2}\frac{e^2 f}{\varepsilon_0 c m_0 n} = n\frac{2\pi}{3\lambda^2}\frac{e^2 f}{\varepsilon_0 c m_0}, \tag{18a}$$

or equivalently,

$$\Gamma_{sp} = 2\gamma_{sp} = \frac{2\pi}{3(\lambda/n)^2}\frac{2\hbar\omega_0\mu_{12}^2}{\hbar^2\varepsilon_0 nc} = \frac{8\pi^2 n}{3\lambda^3}\frac{\mu_{12}^2}{\hbar\varepsilon_0}. \tag{18b}$$

Numerically, the energy broadening (FWHM) due to spontaneous emission is,

$$\hbar\Gamma_{sp}\ (\mu\text{eV}) = 0.0146\frac{nf}{\lambda^2\ (\mu\text{m})}, \tag{19}$$

corresponding to a radiation life time of the exciton

$$\tau_{sp}\ (\text{ns}) = \frac{1}{\Gamma_{sp}}\ (\text{ns}) = 45\frac{\lambda^2\ (\mu\text{m})}{nf}. \tag{20}$$

For an InAs self-assembled quantum dot [8], $\lambda = 0.970\ \mu\text{m}$, $f = 11.8$ and $n = 3.6$ (for GaAs) from which we determine $\Gamma_{sp} = 0.66\ \mu\text{eV}$ and $\tau_{sp} = 1$ ns. Such small values of the line width have not yet been achieved. Instead, in this experiment the line width was found to be 2 μeV, larger than the limit for radiation dephasing, but still the smallest yet recorded for a semiconductor quantum dot. The dephasing is most likely dominated by acoustic phonon scattering at 4 K, the temperature at which the experiments were carried out.

The limit of radiation broadening determines the maximum possible resonant absorption. Substituting the relaxation rate γ_{sp} into the expression for the absorption strength (Eq. (10)), we obtain α_{sp}, the absorption at the resonance for a radiation damped exciton,

$$\alpha_{sp} = \frac{3}{2\pi}\frac{(\lambda/n)^2}{A}. \tag{21}$$

Remarkably, the above expression shows that when the dephasing is dominated by radiation damping, the maximum contrast in the transmission and reflectivity spectra no longer depends on the oscillator strength f. When the driving laser has a Gaussian beam profile of diameter ϕ_{FWHM} measured at half maximum intensity, the illumination area A is given by,

$$A \cong 1.13\phi_{\text{FWHM}}^2. \tag{22}$$

So, assuming that the dot is placed at the center of the illuminated spot, the numerical value of the maximum absorption contrast for such an experiment is given by,

$$\alpha_{sp} \cong 0.423\left(\frac{\lambda}{n\phi_{\text{FWHM}}}\right)^2. \tag{23}$$

For the case of a quantum dot emitting at $\lambda = 0.970\ \mu\text{m}$, beam-width of $\phi_{\text{FWHM}} = 1.3\ \mu\text{m}$, and $n = 3.6$ (the GaAs value), values appropriate to the experiment [8], the expected maximum contrast in transmission would be ideally $\alpha_{sp} = 1.82\%$. We remark here that a reduction of the laser spot diameter by a factor of about 3 would increase the strength of the absorption peak to about 20%. This experimental situation has not yet been achieved.

We showed above in the analysis leading to equation Eq. (13) that the product of the maximum absorption and the dephasing rate depends only on the oscillator strength and

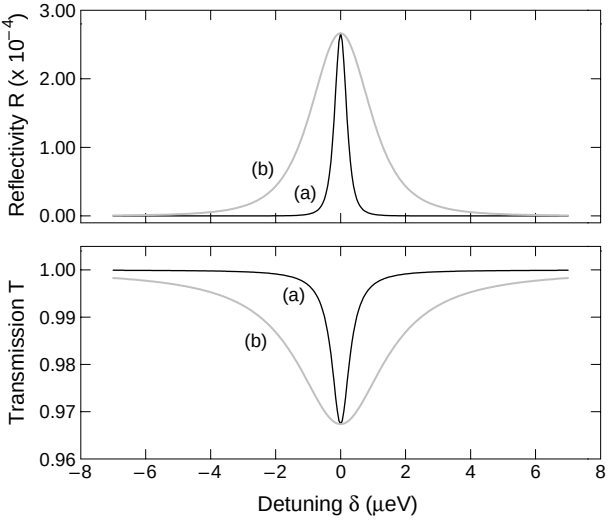

Fig. 2. Calculated transmission and reflectivity for a quantum dot as a function of the photon energy detuning from the ground state exciton resonance. Curves labeled (a) are calculated for an exciton life time of 1 ns, and (b) with a life time of 200 ps. We assumed a Gaussian optical probing spot of 1 μm (FWHM). The optical resonance is assumed at wavelength $\lambda = 1$ μm.

the illumination area. In terms of the width of the resonance,

$$\alpha_{sp}\Gamma_{sp} = \alpha_0\Gamma = \frac{1}{A}\frac{e^2 f}{\varepsilon_0 c m_0 n}, \tag{24a}$$

or equivalently,

$$\alpha_{sp}\Gamma_{sp} = \alpha_0\Gamma = \frac{1}{A}\frac{2\hbar\omega_0\mu_{12}^2}{\hbar^2\varepsilon_0 nc}. \tag{24b}$$

For a Gaussian spot with $A = 1.13\phi_{\mathrm{FWHM}}^2$, the numerical value of the preceding equation is,

$$\alpha_0\hbar\Gamma\ (\mu\mathrm{eV}) = 6.17\times 10^{-3}\frac{f}{n\phi_{\mathrm{FWHM}}^2\ (\mu\mathrm{m})}. \tag{25}$$

Equivalently, the oscillator strength is determined by,

$$f = 162 n\phi_{\mathrm{FWHM}}^2\ (\mu\mathrm{m})\alpha_0\hbar\Gamma\ (\mu\mathrm{eV}). \tag{26}$$

We have recently measured the ground state excitonic resonance with a transmission experiment on a single quantum dot. We find that the maximum absorption is $\alpha_0 = 0.006$ for a Gaussian probing beam with $\phi_{\mathrm{FWHM}} = 1.3$ μm. The measured line width was $\Gamma = 2$ μeV, implying $f = 11.8$, an unambiguous measurement of the oscillator strength.

This analysis is illustrated in Fig. 2 which shows calculated transmission and reflectivity spectra for life time broadened excitons. The illumination assumed is a Gaussian of 1 μm full width at half maximum. It can be seen that in this fundamental limit, the sizes of the

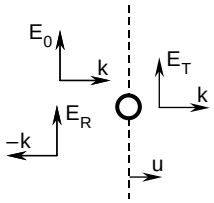

Fig. 3. The electric fields associated with the incident (E_0), transmitted (E_T) and reflected (E_R) waves. The dot plane is shown by a dashed line. **u** is a unit vector along the direction of propagation of the incident beam.

transmission and reflectivity peaks do not depend on the exciton life time. Also the figure shows that the maximum reflectivity contrast is about two orders of magnitude smaller than the contrast seen in the transmission illustrating the point made about the built in homodyne detection in the case of the transmission.

3. Super radiant damping of interacting identical dots

The analysis above can lead to unphysical results when A, the area of the illumination, is decreased. For instance, an examination of Eq. (9) shows that α_0 can exceed the theoretical limit of 100% when A is decreased sufficiently. This highlights the limitations of the approximations made so far. In the model we considered a uniform sheet of dipole oscillators with density $1/A$. When A decreases, the density increases and the quantum dot dipoles inevitably interact with each other. The interaction, a dipole–dipole interaction, has been ignored so far. We consider in this section the transmission of a two-dimensional system of dipoles by solving Maxwell's equations. However, it is clear that this is not the situation depicted in Fig. 1. Instead, by design only one quantum dot is present in the focal point; a system of interacting dipoles is a theoretical construct. In the case of just a single quantum dot interacting with a very tightly focused laser beam, the resolution of the unphysical results from Section 1 is provided only by considering the exact electromagnetic fields [15, 16]. In other words, the assumption of a plane wave is no longer valid for a highly focused beam. As the spot size reduces all the spatial frequencies of the field should be taken into account. This is potentially a complicated calculation, and is beyond the scope of this work. These comments notwithstanding, it is instructive to pursue the case of a plane wave interacting with an array of identical dipoles. In particular, the following results apply for a hypothetical sample containing a high density of dots nearly identical in size where the inhomogeneous broadening in the absorption is small compared to the exciton life time limited radiation broadening.

We assume that all quantum dots in area A are similar enough in size that their excitonic lines are separated by much less than the excitonic line width. We retain the assumption of a plane wave with an array of dots in a two-dimensional plane. This problem bears many resemblances to the cyclotron resonance of a two-dimensional electron system where there is also a dense array of two-dimensional dipoles [17, 18]. We consider the plane wave fields indicated in Fig. 3. The incident electromagnetic field E_0 has the spatial and temporal form $\exp(ikz - i\omega t)$, and drives the exciton resonance in the quantum dots leading to a

transmitted field E_T with wave vector k and a reflected field E_R with wave vector $-k$. The sheet of dots is polarizable and the response of the dots to the driving field amounts to a surface current j_S in the plane of the sheet.

The two continuity equations for the electromagnetic fields at the plane formed by the quantum dots are,

$$\begin{aligned} &\vec{u}\cdot(\vec{E}_0+\vec{E}_R)=\vec{u}\cdot\vec{E}_T,\\ &\vec{u}\times(\vec{H}_0+\vec{H}_R)+\vec{j}_S=\vec{u}\times\vec{H}_T, \end{aligned} \tag{27}$$

where u is a unit vector perpendicular to the two-dimensional plane of dots and oriented along the direction of propagation of the incident beam. Using Maxwell's equation,

$$\vec{\nabla}\times\vec{E}=-\mu_0\partial\vec{H}/\partial t, \tag{28}$$

along with the plane wave form of the fields we find,

$$i\vec{k}\times\vec{E}=i\omega\mu_0\vec{H}. \tag{29}$$

The continuity equations are then,

$$\begin{aligned} &\vec{E}_0+\vec{E}_R=\vec{E}_T,\\ &\vec{u}\times(\vec{k}\times\vec{E}_T-\vec{k}\times\vec{E}_0-\vec{k}\times\vec{E}_R)=\omega\mu_0\vec{j}_S. \end{aligned} \tag{30}$$

In the context of a linear response theory, we assume that the surface current density is linearly proportional to the total field in the dot plane,

$$\vec{j}_S=\sigma\vec{E}_T, \tag{31}$$

where σ is the dynamic conductivity, which, as we show, is related to the polarizability. The system of equations now reduces to,

$$\begin{aligned} &\vec{E}_0+\vec{E}_R=\vec{E}_T,\\ &\vec{E}_0+\vec{E}_R-\vec{E}_T=-\sigma_S/(\varepsilon_0 cn)\vec{E}_T, \end{aligned} \tag{32}$$

and can be solved for the transmittance and reflectance coefficients t and r defined as,

$$t=\frac{E_T}{E_0},\qquad r=\frac{E_R}{E_0}. \tag{33}$$

The results are,

$$t=\frac{1}{1+\sigma_S Y},\qquad r=-\frac{\sigma_S Y}{1+\sigma_S Y}, \tag{34}$$

where $Y=1/(2\varepsilon_0 cn)$ is the impedance of the medium to an electromagnetic wave. The transmission and reflectivity coefficients are related to t and r by,

$$T=tt^*\qquad\text{and}\qquad R=rr^*. \tag{35}$$

The surface current is given by both $j_S=(-e)A\mathrm{d}r/\mathrm{d}t$ and $j_S=\sigma_S E$. The velocity $\mathrm{d}r/\mathrm{d}t$ was given above in Eq. (4), allowing us to deduce an equation for the dynamic

conductivity,

$$\sigma_S = \frac{e^2 f}{Am_0} \frac{-i\omega}{\omega_0^2 - \omega^2 - i\omega\Gamma}. \tag{36}$$

Assuming, as in Section 1, that the exciton transitions are sharp, namely that $\Gamma \ll \omega_0$ which is clearly the case at cryogenic temperatures, the conductivity simplifies to,

$$\sigma_S \cong \frac{e^2 f}{Am_0} \frac{-i\omega_0}{2\omega_0(\omega_0 - \omega) - i\omega_0\Gamma}, \tag{37}$$

which can be conveniently expressed in real and imaginary parts as,

$$2Y\sigma_S \cong \alpha_0 \frac{\gamma^2}{\delta^2 + \gamma^2} + i\alpha_0 \frac{\delta\gamma}{\delta^2 + \gamma^2}. \tag{38}$$

Calculating $T = tt^*$ we obtain,

$$T = \frac{(\omega_0 - \omega)^2 + \gamma^2}{(\omega_0 - \omega)^2 + (\Omega_{SR} + \gamma)^2}, \tag{39}$$

where,

$$\Omega_{SR} = \frac{1}{4A} \frac{e^2 f}{\varepsilon_0 c m_0 n} = \frac{\alpha_0}{2}\gamma. \tag{40}$$

Eq. (39) should be compared with the results from Section 1, Eq. (17). It can be seen that the new result describes a Lorentzian-shaped transmission resonance but with an increased line width. The increase in the line width arises from the continuity equations of the electromagnetic fields at the interface, equivalently from the dipole–dipole interactions in the plane. Similarly, the new expression for the reflectivity is,

$$R = \frac{\Omega_{SR}^2}{(\omega_0 - \omega)^2 + (\Omega_{SR} + \gamma)^2}. \tag{41}$$

The absorption Abs is determined from energy conservation, $\text{Abs} + T + R = 1$, giving,

$$\text{Abs} = \frac{2\Omega\gamma}{(\omega_0 - \omega)^2 + (\Omega + \gamma)^2}. \tag{42}$$

The above results for T, R and Abs can also be expressed by using the definition of Ω_{SR} in Eq. (40):

$$\begin{aligned} T &= 1 - \frac{\alpha_0\gamma^2(1 + \alpha_0/4)}{\delta^2 + \gamma^2(1 + \alpha_0/2)^2} \\ R &= \frac{\alpha_0^2\gamma^2/4}{\delta^2 + \gamma^2(1 + \alpha_0/2)^2} \\ \text{Abs} &= \frac{\alpha_0\gamma^2}{\delta^2 + \gamma^2(1 + \alpha_0/2)^2}. \end{aligned} \tag{43}$$

When $\alpha_0 \ll 1$, these results are identical to the ones derived in Section 1. Deviations arise when α_0 becomes large. In fact, in the limit of large α_0, we have $T = 0$, $R = 1$ and Abs

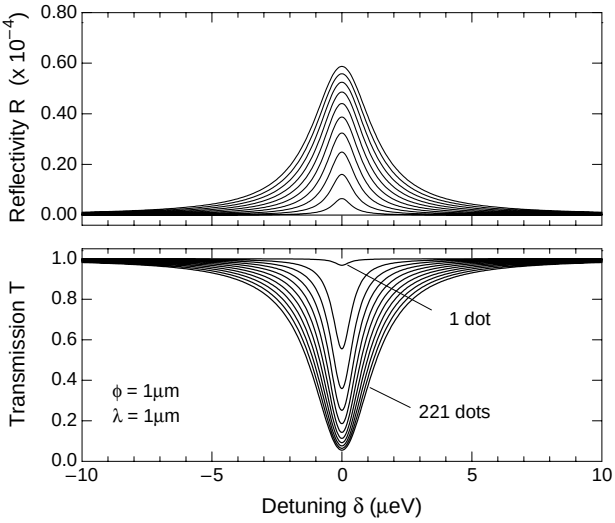

Fig. 4. Transmission and reflectivity as a function of the photon energy detuning from the exciton resonance. The number of identical dots illuminated in the probing optical spot in increased from 1 to 221 in steps of 20. We assumed a Gaussian spot size of FWHM of 1 μm such that the maximum density of dots corresponds to $2.2 \times 10^{10}/\mathrm{cm}^2$. We assumed an exciton absorption wavelength $\lambda = 1$ μm.

vanishes like $4/\alpha_0$. In contrast to the results in Section 1, the solutions are well behaved in the limit of large α_0.

The transmission and absorption have Lorentzian-shaped resonances with FWHM $= \Gamma(1 + \alpha_0/2)$. The new relaxation rate is larger than the intrinsic dot radiation damping rate Γ by factor $(1 + \alpha_0/2)$. This width enhancement is negligible when $\alpha_0 \ll 1$, a case which is representative of current experiments. However, when $\alpha_0 \gg 1$, the line width is equal to $\Gamma\alpha_0/2$ which scales as f/A, namely with the density of quantum dots in the sheet and the oscillator strength of the dot. This gives the clue to the origin of the broadening mechanism: it arises through a coherent coupling of the dipoles, and is a manifestation of super radiance.

Fig. 4 illustrates the resonances obtained in transmission and reflectance from identical dots located in a 1 μm wide Gaussian optical spot. As the number of identical dots is increased, the amplitude of the resonances increases. At the same time, the resonances broaden due to super radiance.

As a final comment on the analysis of transmission and reflectivity from a quantum dot in a homogeneous medium, we note that implicit in the analysis so far is the assumption that the transmission and reflectivity measurements are not influenced by the light re-emitted by the quantum dot, the scattered light. This is no longer true when the numerical aperture of all the lenses in the optical system approaches 1. If the exciton dephasing is limited by radiation, there cannot be any significant non-radiative processes, so that every absorbed photon will eventually be re-emitted. In a CW experiment, both original laser photons and scattered photons contribute to the reflectivity and transmission signals,

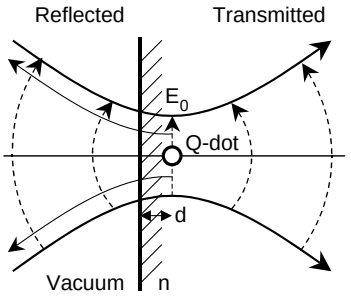

Fig. 5. Schematic view of a quantum dot near the sample surface. The focused laser beam is assumed to have a depth of field much larger than the separation between the quantum dot and the semiconductor surface so that the electromagnetic field can be approximated with a plane wave both in the quantum dot plane and at the sample surface.

changing the expected contrast in the transmission and reflectivity. Assuming that the power is low so that spontaneous re-emission dominates over stimulated emission, the re-emitted photons are equally likely to be detected by the transmission and reflectivity photo detectors. Under these conditions, we expect new values T_{CW} and R_{CW} for the transmission and reflectivity given by,

$$T_{CW} = T + \mathrm{Abs}/2 \qquad \text{and} \qquad R_{CW} = R + \mathrm{Abs}/2. \tag{44}$$

As expected, $T_{CW} + R_{CW} = 1$ and $\mathrm{Abs}_{CW} = 0$. In this scenario, the contrast in the transmission at resonance is very small. While present experiments are far from this limit (the effective numerical aperture in the semiconductor is 0.15 in our experiment [7–9]), this point should be borne in mind as attempts are made to decrease the spot size.

4. Surface proximity effects

Up until now, the dot was considered to be embedded in a homogeneous medium with optical index n. This is not the typical case in practice. In most samples, the dot is located a small distance d beneath the sample surface. Typically, d ranges from 10 to several 100 nm. In this case, the back-scattered light from the dot now adds coherently to the reflected light from the sample surface. We show now that such an effect can modify substantially the intensity and the resonance line shape of the reflected signal. In addition, we find the free surface has also a significant effect on the transmitted signal.

The experimental configuration is shown schematically in Fig. 5. We retain the approximation that near the focus, the fields can be considered in a first approximation as plane waves. We need to calculate the transmittance $t = E_T/E_0$ and the reflectance $r = E_R/E_0$ of the plane waves shown in Fig. 6. To do this, we employ the formalism explained in [19]. This formalism, based on optical transfer matrices, rigorously takes account of the multiple reflections between the dot layer and the sample surface. The details of this calculation are given in Appendix A. In the experiments [4–9], a differential technique is employed by switching the dot absorption on and off either by the Stark effect or by Pauli

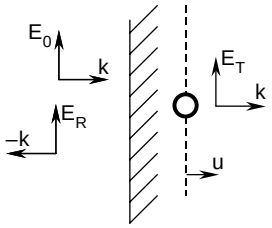

Fig. 6. The electromagnetic waves appropriate to the situation in Fig. 3, assuming plane waves.

blocking. To model the experiments, we therefore calculate the transmission (reflectivity) contrast, the difference between the transmission (reflectivity) with and without the exciton resonance normalized to the transmission (reflectivity) without the exciton resonance. For the transmission the result is,

$$\frac{\Delta T}{T} \cong -\alpha_0 \frac{\gamma^2}{\delta^2+\gamma^2}\left[1-\frac{1-n}{1+n}\left(\cos 2\varphi + \frac{\delta}{\gamma}\sin 2\varphi\right)\right], \tag{45}$$

where $\varphi = 2\pi nd/\lambda$ is the phase shift between a wave reflected from the sample surface and one reflected from the dot layer. For $n = 1$, we recover our previous result as in this case the dot is located in a homogeneous medium, namely the vacuum. However, for $n > 1$ which is the case in the experiments, the transmission contrast is modified by the second term, a consequence of the interference between the dot layer and the surface. The interference depends on the dot to surface separation d through the phase term φ. This changes both the transmission line shape and the contrast at zero detuning. For a dot located at the sample surface, i.e. $d = 0$, the resulting transmission mimics that of a dot in a homogeneous medium with index $(n + 1)/2$, a result we used to analyze our ensemble measurements [4]. For non-zero d, the transmission contrast depends significantly on the interference term. For instance, in the particular case of $\cos 2\varphi = \pm 1$, the line shape is still a symmetric Lorenzian but with a modified amplitude:

$$\frac{\Delta T}{T} \cong -\left(1 \pm \frac{1-n}{1+n}\right)\alpha_0 \frac{\gamma^2}{\delta^2+\gamma^2} \qquad \text{for } \cos 2\varphi = \pm 1. \tag{46}$$

Since $n = 3.6$ for GaAs, we see that the amplitude of the differential transmission can vary between 0.44 and 1.56 times the result for a dot completely buried in GaAs. This point must be carefully considered when one determines the dot oscillator strength from the measured data. In the worst case, an error in d can lead to an error larger than 300% in the oscillator strength.

A similar analysis can be made for the differential reflectivity. We find that,

$$\frac{\Delta R}{R} \cong \frac{4n}{n^2-1}\alpha_0 \frac{\gamma^2}{\delta^2+\gamma^2}\left(\cos 2\varphi - \frac{\delta}{\gamma}\sin 2\varphi\right). \tag{47}$$

In the case of a buried dot, the reflectivity contrast was the square of the transmission contrast, and therefore very small. Now that the dot is considered to be close to the

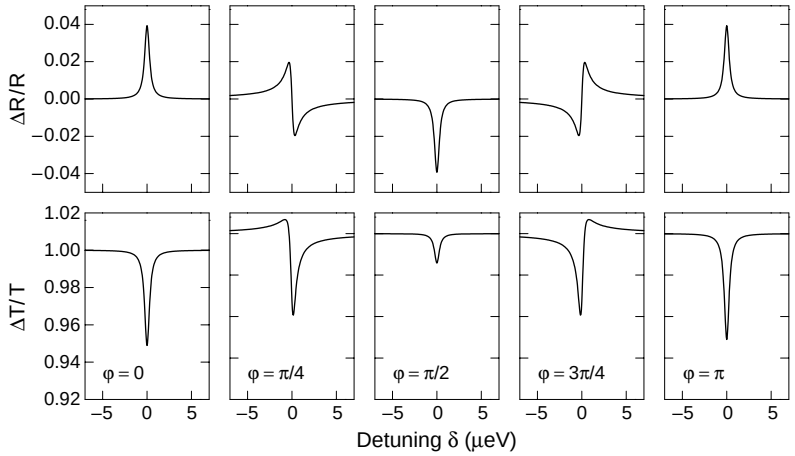

Fig. 7. Transmission and reflectivity as a function of the photon energy detuning from the exciton resonance for five different values of d, the distance between the quantum dot and the sample surface. The phase $\varphi = 2\pi dn/\lambda$ relates this distance d to the exciton optical transition wavelength and the sample optical index n. We assumed a Gaussian spot size of FWHM of 1 μm and $\lambda = 1$ μm with radiation broadening corresponding to an exciton life time of 1 ns.

surface, Eq. (47) demonstrates that the reflectivity contrast is much increased, and is in fact comparable to the contrast in transmission. For example,

$$\frac{\Delta T}{T} \cong -\frac{n-1}{2}\frac{\Delta R}{R} \text{ for } \cos 2\varphi = 1 \text{ and } \frac{\Delta T}{T} \cong -\frac{n-1}{2n}\frac{\Delta R}{R} \text{ for } \cos 2\varphi = -1 \quad (48)$$

which show that for $n = 3$ and $\cos 2\varphi = +1$, both transmission and reflectivity resonances are of equal magnitude. The form of the reflectivity signal depends strongly on φ. When $\cos(2\varphi) = \pm 1$, the differential reflectivity has a Lorentzian shape typical to an absorption resonance. Conversely, when $\sin 2\varphi = \pm 1$, the differential reflectivity is purely dispersive. While there are associated changes in the line shape of the differential transmission, the differential transmission retains an absorption character for all φ. These points are illustrated in Fig. 7, which shows calculated transmission and reflectivity of a quantum dot with a life time limited exciton transition. The calculated data are obtained for dots placed at different distances from the sample surface. A clear feature is that the differential reflectivity can be made to follow either the real part or the imaginary part of the excitonic polarizability depending on the value of d. This illustrates the point that by controlling the phase difference between the interfering waves, it is possible to access experimentally the full permittivity tensor.

5. Interferometry of a single quantum dot

The above section demonstrates that the results, particularly for the reflectivity, are particularly dependent on the optical path difference between the quantum dot and the sample surface. It is difficult to vary this optical path in an experiment, making it difficult

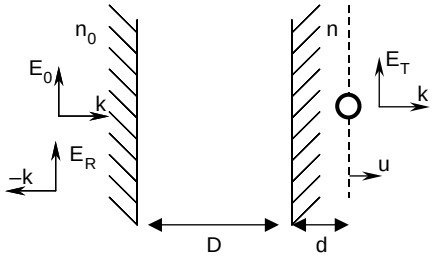

Fig. 8. Schematics of the plane wave approximation for a quantum dot positioned behind a Fabry–Perot etalon. The two mirrors of the etalon are the dielectric–vacuum interface and the vacuum–semiconductor interface.

to exploit the idea of using the reflectivity to determine both the real and imaginary parts of the polarizability. An alternative is to consider the sample as forming one mirror of a Fabry–Perot cavity. The other mirror of the cavity can be some distance away, and can be simply an air–dielectric interface. The idea is that both the laser wavelength and the dot resonance can be tuned through the resonances of the Fabry–Perot cavity. The physics of the problem, sketched schematically in Fig. 8, remain very similar to that in Section 4 except that it is no longer possible to express the differential transmission and reflectivity with simple formulae. Analytical results are still possible however. After a lengthy calculation given in Appendix B, we obtain the following results for the differential reflectivity and transmission coefficients,

$$\frac{\Delta T}{T} \cong -\alpha_0 \frac{\gamma^2}{\delta^2+\gamma^2}\,(1 - G(\varphi,\, \Phi), \tag{49}$$

$$\frac{\Delta R}{R} = \alpha_0 \frac{\gamma^2}{\delta^2+\gamma^2} G(\varphi,\, \Phi) H(\Phi), \tag{50}$$

where the functions G and H are defined as,

$$G(\varphi,\, \Phi) = \left\{(1+r_1^2)r_2\left[\cos 2\varphi - \frac{\delta}{\gamma}\sin 2\varphi\right] + r_1\left[\cos 2(\varphi+\Phi) - \frac{\delta}{\gamma}\sin 2(\varphi+\Phi)\right] + r_1 r_2^2\left[\cos 2(\varphi-\Phi) - \frac{\delta}{\gamma}\sin 2(\varphi-\Phi)\right]\right\} \times \{r_1^2 r_2^2 + 1 + 2r_1 r_2 \cos 2\Phi\}^{-1}$$

and,

$$H(\Phi) = \frac{r_1^2 + r_2^2 - r_1^2 r_2^2 - 1}{r_1^2 + r_2^2 + 2r_1 r_2 \cos 2\Phi},$$

where the first and second interface reflectances are,

$$r_1 = \frac{n_0 - 1}{n_0 + 1} > 0, \qquad r_2 = \frac{1-n}{1+n} < 0. \tag{51}$$

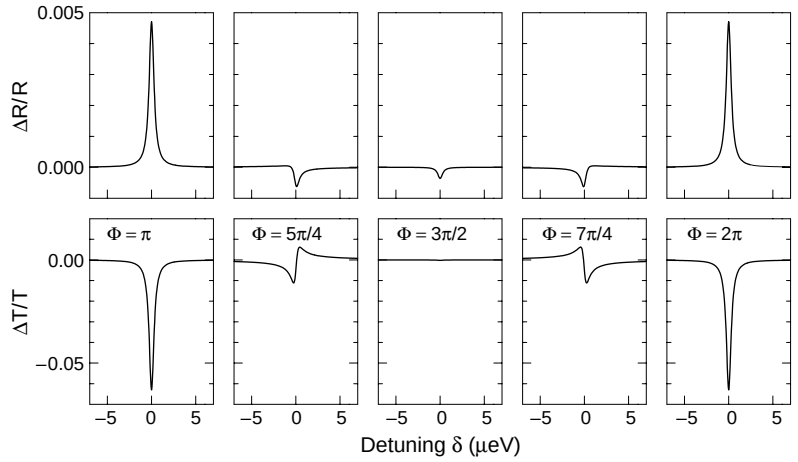

Fig. 9. Interferometry on a single quantum dot. The transmission and reflectivity as a function of the photon energy detuning from the exciton resonance are calculated for five different values of D, the distance between the two mirrors in the Fabry–Perot cavity. The phase $\Phi = 2\pi D/\lambda$ relates this distance to the exciton optical transition wavelength. The phase $\varphi = 2\pi dn/\lambda$ defines the distance of the dot behind the sample surface. We have taken here $\varphi = \pi/2$. The interferometer mirror is assumed to be dielectric and highly reflecting with a reflectivity of 96%. We assumed a Gaussian spot size of FWHM of 1 μm and $\lambda = 1$ μm, and radiation broadening with an exciton life time of 1 ns.

The cavity length D and the distance d between the dot and the sample surface determine the phases,

$$\Phi = \frac{2\pi D}{\lambda} \qquad \text{and} \qquad \varphi = \frac{2\pi dn}{\lambda}. \tag{52}$$

The equations above show that it is possible to perform interferometry on a single quantum dot by adjusting the cavity length D or the laser wavelength, both of which are included in the phase term Φ. Fig. 9 illustrates the behavior of the differential transmission and reflectivity resonances for a single quantum dot for different separations between the mirrors in the Fabry–Perot arrangement. For the parameters chosen here, the transmission exhibits two distinct behaviors, namely, a resonance in the shape of an absorption curve and a resonance in the shape of a dispersion curve. Such an experiment would allow a determination of both the real and imaginary parts of the permittivity of the dot.

6. Saturation of the optical absorption

In the limit of a strong driving field, it is well known that the absorption of a two-level system saturates [13, 14]. The saturation is characterized by a decrease in the absorption at resonance, a decrease in the spectrally integrated absorption intensity and an increase in the line width. The latter effect is referred to as power broadening. We can anticipate the same effects in a quantum dot because, at least in the spectral range close to the exciton resonance, the quantum dot behaves like a two-level system where each state has a

confined, atom-like character. We show here how the saturation behavior can be exploited to determine the Rabi frequency of the ground state exciton in a resonant laser field.

The origin of the saturation lies in the dynamics of the interaction of an exciton with a resonant laser field. Once an exciton has been excited in a quantum dot, the exciton energy will be dissipated. For an excited exciton, the exciton first relaxes to its ground state, and then decays radiatively by spontaneous emission [7]. In this case, the relaxation step takes the exciton out of resonance with the driving laser field. However, for the ground state exciton, there is no relaxation pathway such that the exciton remains in resonance with the laser field. At low laser power, the exciton decays through spontaneous emission. However, at higher laser power, there is an increased chance of decay through stimulated emission. Since the photon originating from stimulated emission is identical to an incoming photon, the process does not contribute to any contrast in differential transmission. This causes the absorption to saturate. Also, the life time of an exciton is decreased by stimulated emission, causing the transmission resonance to broaden. We anticipate that a saturation of the resonance takes place as soon as stimulated emission dominates over spontaneous emission.

The starting point for our analysis of the saturation properties is the result for the optical scattering cross-section, integrated over all angles, as calculated for a two level system from the optical Bloch equations in the rotating wave approximation [13, 14]. The optical scattering cross-section Σ_T is,

$$\Sigma_T = \frac{3(\lambda/n)^2}{2\pi} \frac{\gamma_{sp}^2}{\delta^2 + \gamma_{sp}^2 \left(1 + \frac{\Omega_{R,N}^2}{2\gamma_{sp}^2}\right)}. \tag{53}$$

Here the relaxation rate through spontaneous emission, γ_{sp}, is given in Eqs. (18a) or (18b), and $\Omega_{R,N}$ is the Rabi frequency for an electric field E_N corresponding to N photons:

$$\Omega_{R,N} = \frac{\mu_{12} E_N}{\hbar}. \tag{54}$$

The proportion of scattered photons is given by $\alpha(\delta) = \Sigma/A$ where A is the area of the focused laser beam as introduced previously. We determine the scattering,

$$\alpha(\delta) = \frac{1}{A} \frac{3(\lambda/n)^2}{2\pi} \frac{\gamma_{sp}^2}{\delta^2 + \gamma_{sp}^2 \left(1 + \frac{\Omega_{R,N}^2}{2\gamma_{sp}^2}\right)}. \tag{55}$$

In the idealized model in which the dot is embedded in a homogeneous medium of optical index n, the transmission and the reflectivity are,

$$T = 1 - \alpha(\delta) \qquad \text{and} \qquad R = [\alpha(\delta)/2]^2. \tag{56}$$

Eq. (55) shows how the absorption at the resonance ($\delta = 0$) and the line width of the resonance increase as the Rabi frequency increases. The square of the Rabi frequency is proportional to the laser intensity, resulting in the phenomenon of saturation. In the limit of a very high Rabi frequency, $\alpha(\delta)$ tends to zero and the width of the resonance is proportional to the Rabi frequency.

It is clearly important to calculate $\Omega_{R,N}^2$ as a function of the spot focus geometry and the characteristics of the excitonic dipole. The classical relation between the field amplitude due to N photons and the light power P at quantum dot position is,

$$S = \frac{1}{2}\varepsilon_0 \varepsilon n E_N^2 = \frac{P}{A}. \tag{57}$$

We assume for now a spot focus of area A in which we consider the electric component of the electromagnetic field to be constant. Using $\varepsilon = n^2$ and rearranging the above formula to,

$$E_N^2 = \frac{2P}{\varepsilon_0 nc}\frac{1}{A} = \frac{2\dot{N}\hbar\omega_0}{\varepsilon_0 nc}\frac{1}{A}, \tag{58}$$

where $\dot{N} = \mathrm{d}N/\mathrm{d}t$ is the number of photon flowing in the focused spot. We determine the saturation parameter,

$$\frac{\Omega_{R,N}^2}{2\gamma_{sp}^2} = \frac{\dot{N}}{A}\frac{\hbar\omega_0\mu_{12}^2}{\gamma_{sp}^2\hbar^2\varepsilon_0 nc}. \tag{59}$$

We now make use of Eq. (18b) for γ_{sp},

$$\frac{\Omega_{R,N}^2}{2\gamma_{sp}^2} = \frac{\dot{N}}{A}\frac{3(\lambda/n)^2}{2\pi}\frac{1}{\gamma_{sp}}. \tag{60}$$

Furthermore, making use of α_{sp} in Eq. (21), we find a simple relation for the saturation parameter,

$$\frac{\Omega_{R,N}^2}{2\gamma_{sp}^2} = \frac{\dot{N}}{\gamma_{sp}}\alpha_{sp} \qquad \text{or} \qquad \frac{\Omega_{R,N}}{\Gamma_{sp}} = \frac{1}{2}\sqrt{\frac{\dot{N}\alpha_{sp}}{\Gamma_{sp}}}, \tag{61}$$

showing how the saturation parameter depends on the ratio of the absorption rate in the absence of saturation effects to the rate of spontaneous emission. We can use this expression in the expression for the scattering,

$$\alpha(\delta) = \alpha_{sp}\frac{\gamma_{sp}^2}{\delta^2 + \gamma_{sp}^2(1+\alpha_{sp}\beta)}, \tag{62}$$

where we define a dimensionless saturation coefficient β which is a ratio of the incoming photon flux to the rate of spontaneous emission,

$$\beta = \frac{\dot{N}}{\gamma_{sp}} = 2\frac{\dot{N}}{\Gamma_{sp}}. \tag{63}$$

The maximum scattering at resonance is then,

$$\alpha(0) = \alpha_{\mathrm{Max}} = \frac{\alpha_{sp}}{1+\alpha_{sp}\beta}, \tag{64}$$

and the resonance FWHM is broadened to,

$$\Gamma = 2\gamma_{sp}\sqrt{1+\alpha_{sp}\beta}. \tag{65}$$

The area under the resonance is proportional to the product of peak size and width, so that,

$$\alpha_{\mathrm{Max}}\Gamma = \frac{1}{A}\frac{e^2 f}{\varepsilon_0 c m_0 n}\frac{1}{\sqrt{1+\alpha_{sp}\beta}}, \tag{66}$$

or equivalently,

$$\alpha_{\mathrm{Max}}\Gamma = \frac{1}{A}\frac{2\hbar\omega_0\mu_{12}^2}{\hbar^2\varepsilon_0 nc}\frac{1}{\sqrt{1+\alpha_{sp}\beta}}. \tag{67}$$

The strength of the resonance normalized to its value at low power in the linear response regime is simply given by,

$$\frac{\alpha_{\mathrm{Max}}\Gamma}{(\alpha_{\mathrm{Max}}\Gamma)_0} = \frac{1}{\sqrt{1+\alpha_{sp}\beta}}. \tag{68}$$

Since β is proportional to the laser intensity we see that the total scattered intensity integrated over frequency decreases like the inverse square root of the laser intensity. The term $\alpha_{sp}\beta$ governs the saturation of the optical transition. So let us express it in terms of the oscillator strength of the exciton and the laser power density outside the sample P_0/A. We find,

$$\alpha_{sp}\beta = \frac{9}{4\pi^3}\frac{\varepsilon_0 m_0}{\hbar e^2 f} n \left(\frac{2n}{n+1}\right)^2 \left(\frac{\lambda}{n}\right)^5 \frac{P_0}{A}, \text{ where we used } \dot{N} = \frac{4n}{(n+1)^2}\frac{P_0}{\hbar\omega}. \tag{69}$$

This expression shows that for a given power density, saturation (i.e. $\alpha_{sp}\beta \gg 1$) is easily reached for a transition with a small oscillator strength in a medium with a high optical index n. The expression is very sensitive to λ so quantum dots emitting at long wavelength will tend to saturate much more rapidly than those emitting at short wavelength.

Fig. 10 illustrates the calculated changes in the resonance peak amplitude and its width for the life time limited resonant ground state excitonic transition of a single quantum dot subjected to increasing laser power densities.

7. A quantum dot in an ideal cavity

Should the dot be confined in a perfect cavity, the value of the Rabi frequency used in the analysis can be considerably enhanced. We estimate $\Omega_{R,N}$ as a function of cavity size for the interacting photon two-level system. Here again the starting point is the relation of the Rabi frequency to the light field experienced by the exciton, Eq. (64). In a cavity, the total average electromagnetic energy is given by,

$$\tfrac{1}{2}\int (\varepsilon_0\varepsilon|\vec{E}(\vec{r})|^2 + \mu^{-1}|\vec{B}(\vec{r})|^2)\mathrm{d}\vec{r} = \hbar\omega(N+1/2), \tag{70}$$

where N is the number of photons confined in the cavity. The case $N = 0$, that is when the cavity is empty of photons, still leads to a finite Rabi energy due to the coupling of the

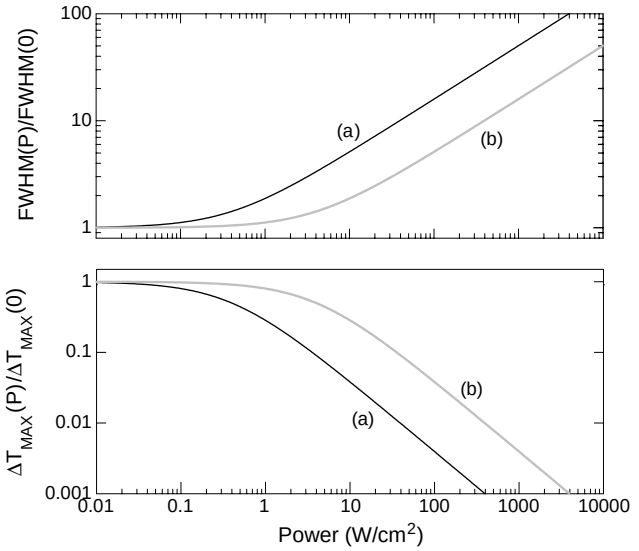

Fig. 10. *Lower panel*: power saturation of the differential transmission peak size as a function of incident photon power density. The data are normalized to the maximum differential transmission for $P = 0$. The power density indicated here is in vacuum outside the medium in which the dot is embedded (here $n = 3.6$). Curve (a) is calculated for an exciton life time of $\tau = 1$ ns with an optical emission wavelength of 1 μm, (b) is obtained for an exciton life time of 100 ps. *Upper panel*: corresponding power broadening showing the relative change in the full width taken at half maximum of the optical transition resonance.

exciton resonance with the vacuum zero point fluctuations. We equate the field energy with quantized photon energy assuming a one-dimensional Fabry–Perot ideal cavity,

$$\int \varepsilon_0 \varepsilon |\vec{E}_N|^2 \cos^2 \frac{2\pi z}{L_z} \mathrm{d}x\mathrm{d}y\mathrm{d}z = \hbar\omega_0 (N + 1/2). \tag{71}$$

We assume a cavity volume $V = AL_z$ where L_z is the cavity length and A is its in-plane area. The field experienced by the dot located in an electric field maximum is then,

$$E_N^2 = \frac{2(N + 1/2)\hbar\omega_0}{\varepsilon_0 \varepsilon} \frac{1}{AL_z}, \tag{72}$$

so that,

$$\frac{\Omega_{R,N}^2}{2} = \frac{\mu_{12}^2}{\hbar^2} \frac{(N + 1/2)\hbar\omega_0}{\varepsilon_0 \varepsilon} \frac{1}{AL_z}. \tag{73}$$

Making use of Eqs. (18) and (21), we find the simple relation,

$$\frac{\Omega_{R,N}^2}{2} = (2N + 1)\alpha_{sp}\gamma_{sp}\nu, \tag{74}$$

where ν is the oscillation frequency of the photon reflected back and forth along the

cavity axis:

$$\nu = \frac{c/n}{2L_z}. \tag{75}$$

We see that the square of the Rabi frequency is proportional to the number of photons N present in the cavity and to the product of the spontaneous radiation rate divided by the time it takes the photon to cross the cavity. We can now evaluate the contribution to the line broadening and maximum scattering intensity due to the Rabi frequency generated by N photons in the focal spot,

$$\frac{\Omega_{R,N}^2}{2\gamma_{sp}^2} = \alpha_{sp}\beta = (2N+1)\alpha_{sp}\frac{\nu}{\gamma_{sp}}. \tag{76}$$

Let us consider the case of a loss-less cavity with a length $L_z = 1$ μm, devoid of photons ($N = 0$), embedded in a medium of optical index $n = 3.6$. For a lateral area of the cavity of about 1 μm^2 and an exciton oscillator strength of about 12, $\alpha_{sp} = 0.001$. The corresponding radiative recombination rate is then $2\gamma = 10^9$/s. We determine for the above set of parameters that $\alpha_{sp}\beta_{sp} = 30$ showing that vacuum quantum fluctuations alone can lead to a very large Rabi frequency. In this particular case it corresponds to 5.5 times the natural line width of the ground state exciton resonance. In the limit of strong coupling the resonant scattering line width is given by,

$$\text{FWHM} = 2\sqrt{(2N+1)\alpha_{sp}\frac{\nu}{\gamma_{sp}}}, \tag{77}$$

and the peak scattering is,

$$\alpha_{\text{Max}} = \frac{1}{\beta} = \frac{1}{(2N+1)}\frac{\gamma}{\nu}. \tag{78}$$

It is an outstanding challenge to demonstrate these results experimentally.

8. Conclusions

We have presented an analytical framework with which absorption experiments on single quantum dots can be understood and interpreted. In particular, we have shown how the dephasing rate can be determined from the line width and how the oscillator strength can be determined from the integrated area of the resonance. In the determination of the oscillator strength, the proximity of the dot to the semiconductor surface must be taken into account as we find significant interference effects between the surface-reflected and quantum dot-reflected plane waves. The interference is particularly marked in the reflectivity which can have either an absorptive or a dispersive line shape depending on the nature of the interference. While it is not obvious how to vary the nature of this interference in an experiment on a particular quantum dot, we suggest an alternative. By positioning the dot just outside a Fabry–Perot cavity, we show how the phase difference between the quantum dot reflectance and the cavity mode can be controllably changed by varying the

cavity length. This experiment should allow interferometry to be performed on a single quantum dot.

A very significant point for a single quantum dot experiment is that the absorption becomes non-linear at a modest power density. We show that this leads to a saturation behavior in the absorption and an increase in the line width. Quantitatively, these effects depend on the Rabi frequency. Finally, we comment that the Rabi frequency can be considerably enhanced by positioning the quantum dot in the anti-node of the electric field distribution in a micro-cavity.

Acknowledgements

We gratefully acknowledge the contributions of our co-workers Alexander Högele, Benito Alén and Pierre Petroff to this work. The work was funded by the DFG under project number SFB 631, the Bavarian-Californian Technology Center and by the EPSRC, UK.

Appendix A

We calculate the transmittance $t = E_T/E_0$ and the reflectance $r = E_R/E_0$ of the electric fields for the situation shown in Fig. 4. We use the formalism of [19] based on optical transfer matrices. In this approach, the electric field in each element is represented by a vector consisting of two elements, the forward and backward propagating plane waves. A 2×2 matrix propagates this vector through the structure. Ref. [19] gives the matrix elements for any layered system including two-dimensional dynamic conductivities at their interfaces.

In the case in Fig. 4, the optical transfer matrix is,

$$\begin{bmatrix} E_0 \\ E_R \end{bmatrix} = \begin{bmatrix} m_{11} & m_{12} \\ m_{21} & m_{22} \end{bmatrix} \begin{bmatrix} E_T \\ 0 \end{bmatrix}. \tag{A1}$$

From the above matrix one deduces immediately that,

$$\begin{aligned} \frac{E_T}{E_0} &= \frac{1}{m_{11}} = t \\ \frac{E_R}{E_0} &= \frac{m_{21}}{m_{11}} = r. \end{aligned} \tag{A2}$$

The transmission and the reflectivity of the sample are given by $T = tt^*$ and $R = rr^*$ so we only need to determine the matrix elements m_{11} and m_{21}. We have two interfaces to consider, namely that of the sample surface and that of the dot-layer. For this reason, the matrix $[m_{ij}]$ is a product of two matrices, one for the semiconductor ($[a_{ij}]$) and one for the dot layer ($[b_{ij}]$). The matrix elements are:

$$\begin{aligned} a_{11} &= \mathrm{e}^{-i\varphi}(1+n)/2 \qquad & b_{11} &= 1+\sigma Y \\ a_{12} &= \mathrm{e}^{+i\varphi}(1-n)/2 \qquad & b_{12} &= +\sigma Y \\ a_{11} &= \mathrm{e}^{-i\varphi}(1-n)/2 \qquad & b_{21} &= -\sigma Y \\ a_{11} &= \mathrm{e}^{+i\varphi}(1+n)/2 \qquad & b_{11} &= 1-\sigma Y \end{aligned} \tag{A3}$$

where, as before, $\varphi = 2\pi nd/\lambda$ and $Y = 1/(2n\varepsilon_0 c)$. We find,

$$t = \frac{1}{m_{11}} = \frac{1}{a_{11}b_{11} + a_{12}b_{21}} = \frac{1}{a_{11}} \frac{1}{1 + \sigma Y(1 - a_{12}/a_{11})}. \tag{A4}$$

In the absence of dot absorption we set $\sigma = 0$ which implies $t = t_0 = 1/a_{11}$, and the relative transmission is,

$$\frac{t}{t_0} = \frac{1}{1 + \sigma Y(1 - a_{12}/a_{11})} \cong 1 - \sigma Y(1 - a_{12}/a_{11}), \tag{A5}$$

where we have assumed a weak absorption, $\sigma Y \ll 1$. The transmission is therefore,

$$\left|\frac{t}{t_0}\right|^2 \cong 1 + 2\sigma_1 Y\,[\mathrm{Re}(a_{12}/a_{11}) - 1] - 2\sigma_2 Y \mathrm{Im}(a_{12}/a_{11}), \tag{A6}$$

where σ_1 and σ_2 are the real and imaginary part of the dot dynamical conductivity. The differential transmission is given by,

$$\frac{\Delta T}{T} = \frac{T(\sigma) - T(0)}{T(0)} = \left|\frac{t}{t_0}\right|^2 - 1. \tag{A7}$$

Using,

$$\frac{a_{12}}{a_{11}} = \mathrm{e}^{2i\varphi} \frac{1 - n}{1 + n}, \tag{A8}$$

we determine,

$$\frac{\Delta T}{T} \cong -2\sigma_1 Y + \frac{n - 1}{n + 1} 2Y\,[\sigma_2 \sin 2\varphi - \sigma_1 \cos 2\varphi]\,. \tag{A9}$$

From the results for the conductivity of a two level system,

$$2Y\sigma_1 \cong \alpha_0 \frac{\gamma^2}{\delta^2 + \gamma^2} \qquad \text{and} \qquad Y\sigma_2 \cong \alpha_0 \frac{\delta\gamma}{\delta^2 + \gamma^2}, \tag{A10}$$

we obtain our final result for the differential transmission,

$$\frac{\Delta T}{T} \cong -\alpha_0 \frac{\gamma^2}{\delta^2 + \gamma^2} \left[1 - \frac{1 - n}{1 + n} \left(\cos 2\varphi + \frac{\delta}{\gamma} \sin 2\varphi\right)\right]. \tag{A11}$$

A similar analysis can be made for the differential reflectivity. For this we have first to determine the reflectance of the system:

$$r = \frac{m_{21}}{m_{11}} = \frac{a_{21}b_{11} + a_{22}b_{21}}{a_{11}b_{11} + a_{12}b_{21}} = \frac{a_{21}}{a_{11}} \frac{1 + \sigma Y(1 - a_{22}/a_{21})}{1 + \sigma Y(1 - a_{12}/a_{11})}. \tag{A12}$$

In the absence of dot absorption, the reflectance of the sample is $r_0 = a_{21}/a_{11}$. The reflectance relative to r_0 is then,

$$\frac{r}{r_0} = \frac{1 + \sigma Y(1 - a_{22}/a_{21})}{1 + \sigma Y(1 - a_{12}/a_{11})} \cong 1 - \sigma Y(a_{12}/a_{11} - a_{22}/a_{21}), \tag{A13}$$

where we again assume $\sigma Y \ll 1$. The relative reflectivity is,

$$\left|\frac{r}{r_0}\right|^2 \cong 1 + 2Y\left[\sigma_1 \mathrm{Re}\left(\frac{a_{12}}{a_{11}} - \frac{a_{22}}{a_{21}}\right) - \sigma_2 \mathrm{Im}\left(\frac{a_{12}}{a_{11}} - \frac{a_{22}}{a_{21}}\right)\right]. \tag{A14}$$

The differential reflectivity is defined as,

$$\frac{\Delta R}{R} = \frac{R(\sigma) - R(0)}{R(0)} = \left|\frac{r}{r_0}\right|^2 - 1, \tag{A15}$$

so that,

$$\frac{\Delta R}{R} \cong 2Y\left[\sigma_1 \mathrm{Re}\left(\frac{a_{12}}{a_{11}} - \frac{a_{22}}{a_{21}}\right) - \sigma_2 \mathrm{Im}\left(\frac{a_{12}}{a_{11}} - \frac{a_{22}}{a_{21}}\right)\right]. \tag{A16}$$

The term involving the matrix elements is,

$$\frac{a_{12}}{a_{11}} - \frac{a_{22}}{a_{21}} = \left(\frac{1-n}{1+n} - \frac{1+n}{1-n}\right)\mathrm{e}^{2i\varphi} = \frac{4n}{n^2-1}\mathrm{e}^{2i\varphi}, \tag{A17}$$

allowing us to determine the explicit form of the differential reflectivity, namely,

$$\frac{\Delta R}{R} = \frac{4n}{n^2-1} 2Y\left(\sigma_1 \cos 2\varphi - \sigma_2 \sin 2\varphi\right). \tag{A18}$$

Finally this leads to

$$\frac{\Delta R}{R} \cong \frac{4n}{n^2-1}\alpha_0 \frac{\gamma^2}{\delta^2+\gamma^2}\left(\cos 2\varphi - \frac{\delta}{\gamma}\sin 2\varphi\right). \tag{A19}$$

Appendix B

The analysis from Appendix A can be extended to the case shown in Fig. 6, a dot situated beneath a Fabry–Perot etalon. Since we have one more interface to consider, the total optical transfer matrix is a product of three matrices, $[m_{ij}] = [f_{ij}][a_{ij}][b_{ij}]$ where $[f]$ refers to the dielectric–vacuum interface and $[a]$ and $[b]$ are defined in Appendix A. Using the results in [19],

$$\begin{aligned} f_{11} &= \mathrm{e}^{-i\Phi}(n_0+1)/2 \\ f_{12} &= \mathrm{e}^{+i\Phi}(n_0-1)/2 \\ f_{11} &= \mathrm{e}^{-i\Phi}(n_0-1)/2 \\ f_{11} &= \mathrm{e}^{+i\Phi}(n_0+1)/2 \end{aligned} \tag{B1}$$

where $\Phi = 2\pi D/\lambda$. D is the separation between the dielectric–vacuum and vacuum–semiconductor interfaces. As in Appendix A, we determine the transmittance and reflectance using,

$$\begin{aligned} \frac{E_T}{E_0} &= \frac{1}{m_{11}} = t, \\ \frac{E_R}{E_0} &= \frac{m_{21}}{m_{11}} = r, \end{aligned} \tag{B2}$$

where now,

$$\begin{aligned} m_{11} &= f_{11}(a_{11}b_{11} + a_{12}b_{21}) + f_{21}(a_{21}b_{11} + a_{22}b_{21}), \\ m_{21} &= f_{21}(a_{11}b_{11} + a_{12}b_{21}) + f_{22}(a_{21}b_{11} + a_{22}b_{21}). \end{aligned} \tag{B3}$$

Only the elements of $[b_{ij}]$ contain the dot dynamic conductivity:

$$r = \frac{f_{21}a_{11} + f_{22}a_{21} + \sigma Y\{f_{21}(a_{11} - a_{12}) + f_{22}(a_{21} - a_{22})\}}{f_{11}a_{11} + f_{12}a_{21} + \sigma Y\{f_{11}(a_{11} - a_{12}) + f_{12}(a_{21} - a_{22})\}}. \tag{B4}$$

In the absence of a dot resonance, the nominal reflectance is,

$$r_0 = \frac{f_{21}a_{11} + f_{22}a_{21}}{f_{11}a_{11} + f_{12}a_{21}}. \tag{B5}$$

Likewise we determine the transmittance,

$$t = \frac{1}{f_{11}a_{11} + f_{12}a_{21} + \sigma Y\{f_{11}(a_{11} - a_{12}) + f_{12}(a_{21} - a_{22})\}}, \tag{B6}$$

such that in the absence of a dot resonance, the nominal transmittance is,

$$t_0 = \frac{1}{f_{11}a_{11} + f_{12}a_{21}}. \tag{B7}$$

The relative reflectance and transmittance are,

$$\frac{r}{r_0} = \frac{1 + A(\sigma Y)}{1 + B(\sigma Y)} \qquad \text{and} \qquad \frac{t}{t_0} = \frac{1}{1 + B(\sigma Y)}, \tag{B8}$$

where,

$$A = 1 - \frac{f_{21}a_{12} + f_{22}a_{22}}{f_{21}a_{11} + f_{22}a_{21}}, \tag{B9}$$

and,

$$B = 1 - \frac{f_{11}a_{12} + f_{12}a_{22}}{f_{11}a_{11} + f_{12}a_{21}}. \tag{B10}$$

We now use the expression of the matrix elements to determine A and B as a function of the interferometer properties. After some algebra we find,

$$A = 1 - \mathrm{e}^{2i\varphi}\frac{r_1 r_2 \mathrm{e}^{-2i\Phi} + 1}{r_1 \mathrm{e}^{-2i\Phi} + r_2}, \tag{B11}$$

and,

$$B = 1 - \mathrm{e}^{2i\varphi}\frac{r_1 \mathrm{e}^{2i\Phi} + r_2}{r_1 r_2 \mathrm{e}^{2i\Phi} + 1}, \tag{B12}$$

where r_1 and r_2 are the first and second mirror reflectances, respectively,

$$r_1 = \frac{n_0 - 1}{n_0 + 1} > 0 \qquad \text{and} \qquad r_2 = \frac{1 - n}{1 + n} < 0. \tag{B13}$$

We can further develop the expression of A and B. We find,

$$1 - A = \frac{(1 + r_1^2)r_2 + r_1 e^{2i(\varphi+\Phi)} + r_1 r_2^2 e^{2i(\varphi-\Phi)}}{r_1^2 + r_2^2 + 2r_1 r_2 \cos 2\Phi}, \tag{B14}$$

and,

$$1 - B = \frac{((1 + r_1^2)r_2 + r_1 e^{2i(\varphi+\Phi)} + r_1 r_2^2 e^{2i(\varphi-\Phi)}}{r_1^2 r_2^2 + 1 + 2r_1 r_2 \cos 2\Phi}. \tag{B15}$$

In the limit $\sigma Y \ll 1$,

$$\frac{r}{r_0} \cong 1 + A(\sigma Y) - B(\sigma Y) = 1 + \sigma Y(A - B), \tag{B16}$$

allowing after some algebra the differential reflectivity to be calculated as,

$$\frac{\Delta R}{R} = \alpha_0 \frac{\gamma^2}{\delta^2 + \gamma^2} G(\varphi, \Phi) H(\Phi) \tag{B17}$$

where

$$\begin{aligned} G(\varphi, \Phi) = \Bigg\{ & (1 + r_1^2)r_2 \left[\cos 2\varphi - \frac{\delta}{\gamma} \sin 2\varphi \right] + r_1 \left[\cos 2(\varphi + \Phi) \right. \\ & \left. - \frac{\delta}{\gamma} \sin 2(\varphi + \Phi) \right] + r_1 r_2^2 \left[\cos 2(\varphi - \Phi) - \frac{\delta}{\gamma} \sin 2(\varphi - \Phi) \right] \Bigg\} \\ & \times \{ r_1^2 r_2^2 + 1 + 2r_1 r_2 \cos 2\Phi \}^{-1} \end{aligned}$$

and

$$H(\Phi) = \frac{r_1^2 + r_2^2 - r_1^2 r_2^2 - 1}{r_1^2 + r_2^2 + 2r_1 r_2 \cos 2\Phi}.$$

The relative transmission is obtained from the relation for the differential reflectance by setting the function A to 0 (see Eq. (B10))

$$\frac{T(\sigma) - T(0)}{T(0)} \cong -2\sigma_1 Y \mathrm{Re}(B) + 2\sigma_2 Y \mathrm{Im}(B) \tag{B18}$$

allowing us to reach after some algebraic manipulation the final result for the differential transmission,

$$\frac{\Delta T}{T} \cong -\alpha_0 \frac{\gamma^2}{\delta^2 + \gamma^2} (1 - G(\varphi, \Phi)). \tag{B19}$$

References

[1] D. Gammon, D.G. Steel, Phys. Today (2002).
[2] D. Bimberg, M. Grundmann, N.N. Ledentsov, Quantum Dot Heterostructures, Wiley, 1998.
[3] R.J. Warburton, Contemp. Phys. 43 (2002) 351.
[4] R.J. Warburton, C.S. Dürr, K. Karrai, J.P. Kotthaus, G. Medeiros-Ribeiro, P.M. Petroff, Phys. Rev. Lett. 79 (1997) 5282.

[5] J.R. Guest, T.H. Stievater, Xiaoqin Li, Jun Cheng, D.G. Steel, D. Gammon, D.S. Katzer, D. Park, C. Ell, A. Thränhardt, G. Khitrova, H.M. Gibbs, Phys. Rev. B 65 (2002) 241310.
[6] T.H. Stievater, Xiaoqin Li, J.R. Guest, D.G. Steel, D. Gammon, D.S. Katzer, D. Park, Appl. Phys. Lett. 80 (2002) 1876.
[7] B. Alén, F. Bickel, K. Karrai, R.J. Warburton, P.M. Petroff, Appl. Phys. Lett. 83 (2003) 2325.
[8] A. Högele, B. Alén, F. Bickel, R.J. Warburton, P.M. Petroff, K. Karrai, Physica E (2003) (in press).
[9] B. Alén, K. Karrai, R.J. Warburton, F. Bickel, P.M. Petroff, J. Martínez-Pastor, Physica E (2003) (in press).
[10] J.D. Jackson, Classical Electrodynamics, third ed., Section 10.11, John Wiley and Son, New York, 1999.
[11] R.P. Feynman, R.B. Leighton, M. Sands, The Feynman Lectures on Physics, vol. 1, 30–12, Formula 30.19, Addison-Wesley, Reading, 1977.
[12] C. Cohen-Tannoudji, B. Diu, F. Laloe, Quantum Mechanics, Wiley-Interscience, 1996.
[13] R. Loudon, The Quantum Theory of Light, Oxford University Press, Oxford, 1983.
[14] L. Mandel, E. Wolf, Optical Coherence and Quantum Optics, Cambridge University Press, Cambridge, 1995.
[15] B. Richards, E. Wolf, Proc. R. Soc. London Ser. A 253 (1959) 358.
[16] M. Lax, Phys. Rev. A 11 (1975) 1365.
[17] G. Abstreiter, P. Kneschaurek, J.P. Kotthaus, J.F. Koch, Phys. Rev. Lett. 32 (1974) 104.
[18] T. Ando, A.B. Fowler, F. Stern, Rev. Modern Phys. 54 (1982) 437.
[19] K. Karrai, S. Huant, G. Martinez, L.C. Brunel, Solid State Commun. 66 (1988) 355.